Atmos. Chem. Phys. Discuss., 15, 33379–33405, 2015
www.atmos-chem-phys-discuss.net/15/33379/2015/
doi:10.5194/acpd-15-33379-2015

Atmospheric Chemistry and Physics Discussions

Observations and implications of liquid–liquid phase separation at high relative humidities in secondary organic material produced by α-pinene ozonolysis without inorganic salts

L. Renbaum-Wolff[1,a,c,*], M. Song[1,b,*], C. Marcolli[2], Y. Zhang[3,a,c], P. F. Liu[3], J. W. Grayson[1], F. M. Geiger[4], S. T. Martin[3,5], and A. K. Bertram[1]

[1]Department of Chemistry, University of British Columbia, Vancouver, BC, V6T 1Z1, Canada
[2]Marcolli Chemistry and Physics Consulting GmbH, Zurich, Switzerland
[3]School of Engineering and Applied Sciences, Harvard University, Cambridge, Massachusetts 02138, USA
[4]Department of Chemistry, Northwestern University, Evanston, IL 60208, USA
[5]Department of Earth and Planetary Sciences, Harvard University, Cambridge, Massachusetts 02138, USA
[a]now at: Aerodyne Research, Inc, Billerica, MA 01821, USA

[b]now at: Department of Earth and Environmental Sciences, Chonbuk National University, Jeollabuk-do, Republic of Korea
[c]now at: Boston College, Chestnut Hill, MA 02467, USA
[*]These authors contributed equally to this work.

Received: 18 October 2015 – Accepted: 2 November 2015 – Published: 26 November 2015

Correspondence to: A. K. Bertram (bertram@chem.ubc.ca) and
S. T. Martin (scot_martin@harvard.edu)

Published by Copernicus Publications on behalf of the European Geosciences Union.

ACPD
15, 33379–33405, 2015

Abstract

Particles consisting of secondary organic material (SOM) are abundant in the atmosphere. To predict the role of these particles in climate, visibility, and atmospheric chemistry, information on particle phase state (i.e. single liquid, two liquids, solid and so forth) is needed. This paper focuses on the phase state of SOM particles free of inorganic salts produced by the ozonolysis of α-pinene. Phase transitions were investigated both in the laboratory and with a thermodynamic model over the range of < 0.5 % to 100 % relative humidity (RH) at 290 K. In the laboratory studies, a single phase was observed from 0 to 95 % RH while two liquid phases were observed above 95 % RH. For increasing RH, the mechanism of liquid–liquid phase separation (LLPS) was spinodal decomposition. The RH range at which two liquid phases were observed did not depend on the direction of RH change. In the modelling studies at low RH values, the SOM took up hardly any water and was a single organic-rich phase. At high RH values, the SOM underwent LLPS to form an organic-rich phase and an aqueous phase, consistent with the laboratory studies. The presence of LLPS at high RH-values has consequences for the cloud condensation nuclei (CCN) activity of SOM particles. In the simulated Köhler curves for SOM particles, two local maxima are observed. Depending on the composition of the SOM, the first or second maximum can determine the critical supersaturation for activation. The presence of LLPS at high RH-values can explain inconsistencies between measured CCN properties of SOM particles and hygroscopic growth measured below water saturation.

1 Introduction

Particles consisting of secondary organic material (SOM) can account for 20–80 % of the total submicron organic mass concentrations in the atmosphere (Zhang et al., 2007; Jimenez et al., 2009). SOM in the particle phase consists of the low volatility fraction of the oxidized products of biogenic or anthropogenic volatile organic compounds

ACPD
15, 33379–33405, 2015

(Hallquist et al., 2009). To predict the role of SOM particles for climate, visibility and atmospheric chemistry, information on the phase state within individual SOM particles (e.g., one liquid, two liquids, one solid, and so forth) is needed. Particle phase state influences the properties of particles such as cloud condensation nuclei (CCN) properties, optical properties, and interactions with reactive and non-reactive gas phase species (Martin et al., 2000; Raymond and Pandis, 2002; Bilde and Svenningsson, 2004; Zuend et al., 2010; Kuwata and Martin, 2012).

A possible phase transition of SOM particles during relative humidity (RH) cycling is liquid–liquid phase separation (LLPS) (Pankow et al., 2003; Petters et al., 2006). LLPS has also been observed in the laboratory when SOM produced by α-pinene ozonolysis was combined with ammonium sulfate and for other organic systems when mixed with inorganic salts when the average organic oxygen-to-carbon elemental ratios were less than approximately 0.8 (Krieger et al., 2012; You et al., 2014). The presence of the ammonium sulfate causes salting-out of the organic material and the formation of two liquid phases. However, we are not aware of previous laboratory studies focusing on LLPS in SOM in the absence of inorganic salts.

This paper focuses on phase transitions of SOM produced by α-pinene ozonolysis free of inorganic salts. α-Pinene was chosen for the precursor gas for SOM because it is an important contributor to organic particle mass concentrations in the atmosphere, especially in regions such as boreal forests (Cavalli et al., 2006). Phase transitions were investigated both in the laboratory and with a thermodynamic model over the range of < 0.5 to 100 % RH.

ACPD
15, 33379–33405, 2015

2 Methods

2.1 Laboratory studies

2.1.1 Production and collection of secondary organic material

Particles of secondary organic material were produced by α-pinene ozonolysis in a flow tube reactor (Shrestha et al., 2013). Details are described therein. A range of particle mass concentrations was generated (Table 1). At the outlet of the flow tube reactor, particles were collected using one of two different methods.

In the first method, the aerosol from the flow tube reactor was passed through an ozone destruction catalyst (Ozone Solutions, model ODS-2) and carbon filter to remove excess reactants (Sunset Laboratory) and the particles were charged in a bipolar charger (TSI, 3077). A portion of the total flow (1.5 slpm) was sampled into a nanometer aerosol sampler (TSI, Model 3089) where particles were collected by electrostatic precipitation (−10 kV sampler potential) onto a siliconized glass slide (Hampton Research, Canada). In previous work, it was established that the collected particle mass was due to impaction of SOM particles rather than condensation of organic vapors (Liu et al., 2013). This method of collection resulted in submicron particles distributed evenly over the glass slide. Since supermicron particles are needed for the optical microscope experiments (see Sect. 2.1.2), the submicron particles were exposed to water supersaturation conditions to grow and coagulate the particles (Song et al., 2015). Specifically, the slides containing the submicron particles was mounted to a temperature and RH-controlled flow cell, which was coupled to a reflectance microscope, as described previously (Koop et al., 2000; Parson et al., 2004; Pant et al., 2006). The RH in the flow cell was initially set to > 100 % by decreasing the cell temperature to below the dew point temperature. At the initial RH (> 100 %) water condensed on the slides forming large (150–300 µm) droplets by growth and coagulation. The RH was then ramped back to ∼ 98 % by warming the cell back to room temperature, resulting in water evaporating from the droplets. This process of coagulation followed by evapo-

ACPD
15, 33379–33405, 2015

ration resulted in SOM particles with lateral dimensions of 5–30 µm. This method was used to collect samples 1, 6, and 9 in Table 1.

In the second method used to collect particles, the aerosol from the flow tube reactor was passed through an ozone destruction catalyst (Ozone Solutions, model ODS-2) and carbon filter to remove excess reactants (Sunset Laboratory), and then a portion of the total flow (1.5 slpm) was sampled into a single stage impactor (Prenni et al., 2009; Poschl et al., 2010). Within the impactor, particles collected and coagulated on glass slides coated with trichloro(*1H,1H,2H,2H*-perfluorooctyl) silane (Sigma-Aldrich, 97 % purity). The coating procedure, which was described in Knopf (2003), was used to generate a hydrophobic surface. The size of the particles after coagulation on the on the glass slides ranged from 10 to 80 µm in diameter. This method was used to collect sample 2–5, 7, and 8 in Table 1.

2.1.2 Method of determining SOM phase(s)

Hydrophobic substrates containing the supermicron particles were located within a flow-cell with temperature and RH control and coupled to a reflectance microscope (Zeiss, AxioTech, 50× objective) for observation (Koop et al., 2000; Parson et al., 2004; Pant et al., 2006). During experiments, the RH was changed by adjusting the moisture content of the gas flow. The RH was measured with a chilled-mirror hygrometer (General Eastern, model 1311DR), which was calibrated using the deliquescence RH of pure ammonium sulfate particles. During typical experiments, the RH was first set to ∼ 100 %, and then the RH was ramped down at a rate of 0.1–0.3 % RH min^{-1} and images were collected every 5–20 s. After the RH reached ≤ 0.5 % RH, it was ramped up again at the same rate to ∼ 100 %. During the experiments, temperature was constant at 290 ± 1 K. From images recorded while changing the RH, the number of phases present in the SOM was determined.

ACPD
15, 33379–33405, 2015

2.2 Thermodynamic modelling studies

Liquid–liquid equilibria and water uptake were calculated with the methods developed by Zuend et al. (2008, 2010, 2011) and Zuend and Seinfeld (2012, 2013). To calculate activity coefficients of the organic species as a function of the solution composition, the thermodynamic group-contribution model AIOMFAC (Aerosol Inorganic–Organic Mixtures Functional groups Activity Coefficients) developed by Zuend et al. (2008, 2010, 2011) was utilized. To represent SOM from the ozonolysis of α-pinene the oxidation products listed in Table 2 were used. These oxidation products were based on the calculations performed by Zuend and Seinfeld (2012), who used the Master Chemical Mechanism (Jenkin et al., 1997; Saunders et al., 2003) in combination with EVAPORATION (Compernolle et al., 2011) to establish a representative condensed-phase composition of oxidation products from the ozonolysis of α-pinene. Three different mixtures of these oxidation products were used in the current study (see Table 2). The mixtures SOM-high and SOM-low are based on calculations by Zuend and Seinfeld (2012) carried out at 60 % RH yielding particle mass concentrations of 21.86 and 0.81 $\mu g\,m^{-3}$, respectively (see Fig. 4 from Zuend and Seinfeld). The SOM-ox mixture used the same oxidation products as SOM-high and SOM-low mixtures, but the share of the more oxidized products was increased. Water uptake and CCN activation for these mixtures were simulated assuming that all oxidation products remained in the condensed phase without further gas-to-particle partitioning.

In addition to detecting the presence of LLPS, the thermodynamic model was used to predict the hygroscopic growth factor (HGF), CCN activation, and the hygroscopicity parameter (κ), from calculations of hygroscopic growth (κ_{HGF}) and calculations of CCN activation (κ_{CCN}). The hygroscopic growth factor was calculated with the following Eq. (1):

$$\mathrm{HGF(RH)} = \frac{D(\mathrm{RH})}{D_0}, \quad (1)$$

ACPD
15, 33379–33405, 2015

where D(RH) and D_0 represent the wet and the dry diameters of the particles, respectively. The dry diameter D_0 was calculated at 1 % RH. The following equation was used to calculate the κ_{HGF} (Petters and Kreidenweis, 2007; Pajunoja et al., 2015):

$$\kappa_{HGF} = 1 - HGF^3 + \frac{HGF^3 - 1}{\frac{RH}{100\,\%}} e^{\left(\frac{4\sigma_w M_w}{RT\rho_w d_p HGF}\right)}, \quad (2)$$

where σ_w is surface tension of water (0.072 N m^{-1}), M_w is molecular weight of water (18 g mol^{-1}), R is the universal gas constant, T is temperature (298 K), ρ_w is the density of water (1 g cm^{-3}), and d_p is diameter of droplet. The following equation was used to calculate κ_{CCN} (Petters and Kreidenweis, 2007; Pajunoja et al., 2015):

$$\kappa_{CCN} = \frac{4A_{Kelvin}^3}{27 d_c^3 \ln^2 S_c}, \quad (3)$$

where

$$A_{Kelvin} = \frac{4\sigma_w M_w}{RT\rho_w}, \quad (4)$$

and d_c and S_c are the critical diameter and saturation ratio, respectively.

3 Results and discussion

3.1 Observations of LLPS in α-pinene-derived SOM particles: laboratory studies

As the RH was scanned from high values (~ 100 %) to low values (≤ 0.5 %) and in reverse, LLPS in the SOM was clearly visible for RH > 95 %. Example images are shown in Fig. 1. As the RH was increased from < 0.5 to ~ 95 %, no change in the image was

ACPD
15, 33379–33405, 2015

observed and the particles were appeared as a single phase. The light-colored circle in the center of the particle in Panel A is an optical effect of light scattering from a hemispherical uniform particle (Bertram et al., 2011). Above ~ 95 % RH, the particle underwent spinodal decomposition, resulting in two phases (see Fig. 1 and Movie S1 in Supplement). Spinodal decomposition is evident from the formation of the many small inclusions of the second phase throughout the particle (Ciobanu et al., 2009; Song et al., 2012). As the RH was increased above ~ 95 % RH, the inclusions containing the second phase increased in size and coagulated into larger inclusions and eventually formed the inner phase of the particle (see Movie S1). After phase separation, two liquid phases persisted until ~ 100 % RH.

Panel B of Fig. 1 shows the same particle as Panel A, but for experiments using decreasing RH starting from close to 100 % RH. At ~ 98 % RH, the particle contained two liquid phases. As the RH decreased from ~ 98 to ~ 95 %, the volume ratio of the outer phase to the inner phase decreased. Below ~ 95 % RH, the two phases merged into a single phase. As the RH was decreased further to < 0.5 % RH, no abrupt change was observed, indicating the absence of any further phase transitions. Figure 2 shows similar pictures as Fig. 1, except in this case the SOM was generated using a higher particle mass concentration in the flow tube reactor.

Figures 1 and 2 show that there are differences in the process of LLPS and the resulting morphology depending on the direction of the RH change. For increasing RH, spinodal decomposition was identified as the mechanism of phase separation. For decreasing RH, disappearance of phase separation occurred by merging of the two phases.

Experiments were also carried out to determine if the lowest RH at which two phases existed depended on the direction of RH change. Values for the lowest RH at which two phases were observed when increasing and decreasing RH are listed in Table 1 and shown in Fig. 3 (black circles correspond to increasing RH and red circles correspond to decreasing RH). Table 1 and Fig. 3 illustrate that the lowest RH at which two phases were observed did not depend significantly on the direction of RH change. Figure 3

ACPD
15, 33379–33405, 2015

and Table 1 also show that within uncertainties of the measurements, there is no effect of the SOM mass loading in the flow tube reactor on the lowest RH at which two liquid phases were observed.

The behavior observed here for SOM without an inorganic salt is markedly different than observed when SOM is mixed with an inorganic salt. For pure SOM, a single phase is observed at low RH and it is not until high RH that phase separation is observed. When SOM from the ozonolysis of α-pinene was mixed with ammonium sulfate the amount of phase separation increases as the RH decreased (You et al., 2012). This increase in the tendency for phase separation with decreasing RH is due to the salting-out effect. As the RH decreases, the particles lose water to maintain equilibrium with the gas phase and as a result the concentration of the salt in the particle increases leading to an increase in salting-out of organics.

3.2 Observations of LLPS in α-pinene-derived SOM particles: thermodynamic modelling studies

Shown in Fig. 4 are the simulated hygroscopic growth factors for the three different SOM mixtures (SOM-high, SOM-low, SOM-ox) with a dry diameter of 20 µm, which is similar in size to the particles used in the optical microscope experiments. At RH values < 98 % the SOM took up little water. However, when the multicomponent systems consisting of organic substances with different hydrophilicities (i.e. different O : C ratios) were exposed to RH values > 98 % RH, LLPS into an organic-rich phase and an aqueous-phase was observed. At the RH of LLPS, the particles took up a significant amount of water, leading to an almost vertical increase in the hygroscopic growth curve as shown in Fig. 4. For the SOM-high mixture LLPS occurred from 98.9–99.94 % RH as indicated by the red segment on the green line of Fig. 4. When the share of the more hydrophilic substances is increased as is the case for the low SOM loading (SOM-low) with a particle mass concentration of 0.81 µg m^{-3} the onset of LLPS shifted to lower RH and the range of LLPS was increased. In the laboratory experiments, LLPS was observed starting at 95 % RH. This lower onset may be due to more highly oxidized

ACPD
15, 33379–33405, 2015

products produced in the laboratory compared with the oxidation products used in the thermodynamic calculations.

4 Implications

4.1 Cloud condensation nuclei properties

The non-ideal behavior of oxidation products from α-pinene ozonolysis in mixtures with water leads to a miscibility gap at RH > 95 % as demonstrated through both laboratory and thermodynamic modelling. This has consequences for the CCN activity of particles as suggested previously (Petters et al., 2006). Shown in Panel A of Fig. 5 are simulated Köhler curves for SOM particles with dry diameters of 100 nm. The Köhler curves show a sharp increase in the equilibrium water vapor supersaturation above the particles (SS) as the size of the particles increases from 100 nm to roughly 110 nm due to the Kelvin effect when they are still in their organic-rich phase (i.e. low water content state). As the particle size increases from 110 to 200 nm there is a steep decrease in SS as the particles switch from the organic-rich phase to two phases by taking up water from the gas phase. This gives rise to the first maximum in the Köhler curve, which occurs at a wet particle diameter of $D_p \approx 110$ nm for the SOM-high mixture. The second maximum of SS at a wet diameter of $D_p \approx 300$ nm is the regular maximum of the Köhler curve, which occurs when the droplet is dilute and close to solution ideality. When the particle is composed of higher shares of the more hydrophilic substances, the first maximum decreases in height while the second maximum remains constant (see Panel A of Fig. 5). For SOM-high (O : C = 0.472) and SOM-low (O : C = 0.513), the first maximum in the Köhler curve determines the critical supersaturation to overcome the activation barrier. In SOM-ox (O : C = 0.582) the second maximum is higher than the first one and relevant for CCN activation. The height of the second maximum in the Köhler curve is sensitive to the molecular weight of the organic substances the droplet consists of and the droplet's surface tension (e.g. Wex et al., 2007, 2008).

ACPD
15, 33379–33405, 2015

Recently researchers have observed inconsistencies between measured CCN properties of SOM particles and hygroscopic growth measured below water saturation, and several reasons have been put forward to explain these discrepancies (Petters et al., 2006, 2009; Prenni et al., 2007; Juranyi et al., 2009; Good et al., 2010; Massoli et al., 2010; Hersey et al., 2013; Pajunoja et al., 2015). This study shows that such inconsistencies are expected for systems with LLPS when the water uptake at subsaturated conditions represents the hygroscopicity of the organic-rich phase while the barrier for CCN activation can be determined by the second maximum in the Köhler curve when the particles are dilute.

The non-ideality of SOM has also consequences for the applicability of the single parameter κ representation of Köhler theory (Petters and Kreidenweis, 2007). If SOM forms an ideal mixture with water then κ_{HGF} is approximately constant over the whole RH range and κ_{CCN} corresponds well with κ_{HGF} for an organic particle (Petters and Kreidenweis, 2007). However, Panel (B) of Fig. 5 shows that κ_{HGF} for the mixtures SOM-high, SOM-low, and SOM-ox with a dry diameter of 100 nm are not constant over the whole RH range. κ_{HGF} decreases from 0.091–0.116 at 10 % RH to 0.025–0.033 at 90 % RH for the different mixtures. In addition, κ_{CCN} strongly depends on whether the first or the second maximum in the Köhler curve is limiting CCN activation. For SOM-high with $\kappa_{CCN} = 0.009$ and SOM-low with $\kappa_{CCN} = 0.036$ the first maximum is limiting while for SOM-ox with $\kappa_{CCN} = 0.080$ the second maximum is limiting.

The simulated dependence of κ_{HGF} on RH for particles with LLPS corresponds well with the one observed by Pajunoja et al. (2015) for α-pinene OH oxidation products with O : C = 0.45. κ_{CCN} measured by Pajunoja et al. (2015) range from 0.08–0.14 (see their Fig. 1c), which is higher than the range simulated here (0.009–0.080). Their high values suggest that the second maximum in the Köhler curve may have been relevant for CCN activation of the particles they studied. Since solution ideality should be well fulfilled for the growing droplet when it passes through the second maximum of the Köhler curve, the higher κ_{CCN} values measured by Pajunoja et al. (2015) compared to the values determined here might be due to lower average molecular weights of the

ACPD
15, 33379–33405, 2015

SOM investigated by Pajunoja et al. (2015) compared with the ones simulated in this study.

4.2 Optical properties

Brunamonti et al. (2015) showed that LLPS in mixed organic/inorganic salt systems may drive soot inclusions to the near-surface region of particles to minimize the free energy of the system. This redistribution of soot inclusions to the outer liquid phase changes the predicted optical properties. LLPS in mixed organic/inorganic salt systems have also been shown to change the partitioning of semivolatile organics between the particle and gas phase and also to change the uptake of reactive gases (Zuend et al., 2010; Zuend and Seinfeld, 2012). Similar phenomena may occur in particles that undergo liquid–liquid separation in the absence of a salt, such as was observed herein.

The Supplement related to this article is available online at doi:10.5194/acpd-15-33379-2015-supplement.

Acknowledgements. This work was supported by the Natural Sciences and Engineering Research Council of Canada. Support from the US National Science Foundation and the US Department of Energy is also acknowledged. Claudia Marcolli acknowledges the Competence Center Environment and Sustainability of the ETH Domain (CCES) project OPTIWARES for financial support and Andreas Zuend for providing the program to perform the model calculations. The authors would also like to thank Doug Worsnop for enthusiastic and motivating discussions related to the current manuscript.

References

Bertram, A. K., Martin, S. T., Hanna, S. J., Smith, M. L., Bodsworth, A., Chen, Q., Kuwata, M., Liu, A., You, Y., and Zorn, S. R.: Predicting the relative humidities of liquid-liquid phase separation, efflorescence, and deliquescence of mixed particles of ammonium sulfate, organic

ACPD
15, 33379–33405, 2015

material, and water using the organic-to-sulfate mass ratio of the particle and the oxygen-to-carbon elemental ratio of the organic component, Atmos. Chem. Phys., 11, 10995–11006, doi:10.5194/acp-11-10995-2011, 2011.

Bilde, M. and Svenningsson, B.: CCN activation of slightly soluble organics: the importance of small amounts of inorganic salt and particle phase, Tellus B, 56, 128–134, doi:10.1111/j.1600-0889.2004.00090.x, 2004.

Brunamonti, S., Krieger, U. K., Marcolli, C., and Peter, T.: Redistribution of black carbon in aerosol particles undergoing liquid–liquid phase separation, Geophys. Res. Lett., 42, 2532–2539, doi:10.1002/2014gl062908, 2015.

Cavalli, F., Facchini, M. C., Decesari, S., Emblico, L., Mircea, M., Jensen, N. R., and Fuzzi, S.: Size-segregated aerosol chemical composition at a boreal site in southern Finland, during the QUEST project, Atmos. Chem. Phys., 6, 993–1002, doi:10.5194/acp-6-993-2006, 2006.

Ciobanu, V. G., Marcolli, C., Krieger, U. K., Weers, U., and Peter, T.: Liquid–liquid phase separation in mixed organic/inorganic aerosol particles, J. Phys. Chem. A, 113, 10966–10978, doi:10.1021/Jp905054d, 2009.

Compernolle, S., Ceulemans, K., and Müller, J.-F.: EVAPORATION: a new vapour pressure estimation methodfor organic molecules including non-additivity and intramolecular interactions, Atmos. Chem. Phys., 11, 9431–9450, doi:10.5194/acp-11-9431-2011, 2011.

Good, N., Topping, D. O., Duplissy, J., Gysel, M., Meyer, N. K., Metzger, A., Turner, S. F., Baltensperger, U., Ristovski, Z., Weingartner, E., Coe, H., and McFiggans, G.: Widening the gap between measurement and modelling of secondary organic aerosol properties?, Atmos. Chem. Phys., 10, 2577–2593, doi:10.5194/acp-10-2577-2010, 2010.

Hallquist, M., Wenger, J. C., Baltensperger, U., Rudich, Y., Simpson, D., Claeys, M., Dommen, J., Donahue, N. M., George, C., Goldstein, A. H., Hamilton, J. F., Herrmann, H., Hoffmann, T., Iinuma, Y., Jang, M., Jenkin, M. E., Jimenez, J. L., Kiendler-Scharr, A., Maenhaut, W., McFiggans, G., Mentel, Th. F., Monod, A., Prévôt, A. S. H., Seinfeld, J. H., Surratt, J. D., Szmigielski, R., and Wildt, J.: The formation, properties and impact of secondary organic aerosol: current and emerging issues, Atmos. Chem. Phys., 9, 5155–5236, doi:10.5194/acp-9-5155-2009, 2009.

Hersey, S. P., Craven, J. S., Metcalf, A. R., Lin, J., Lathem, T., Suski, K. J., Cahill, J. F., Duong, H. T., Sorooshian, A., Jonsson, H. H., Shiraiwa, M., Zuend, A., Nenes, A., Prather, K. A., Flagan, R. C., and Seinfeld, J. H.: Composition and hygroscopic-

ACPD
15, 33379–33405, 2015

ity of the Los Angeles Aerosol: CalNex, J. Geophys. Res.-Atmos., 118, 3016–3036, doi:10.1002/jgrd.50307, 2013.
Jenkin, M. E., Saunders, S. M., Derwent, R. G., and Pilling, M. J.: Construction and application of a master chemical mechanism (MCM) for modelling tropospheric chemistry, Abstr. Pap. Am. Chem. S, 214, 116-COLL, 1997.
Jimenez, J. L., Canagaratna, M. R., Donahue, N. M., Prevot, A. S. H., Zhang, Q., Kroll, J. H., DeCarlo, P. F., Allan, J. D., Coe, H., Ng, N. L., Aiken, A. C., Docherty, K. S., Ulbrich, I. M., Grieshop, A. P., Robinson, A. L., Duplissy, J., Smith, J. D., Wilson, K. R., Lanz, V. A., Hueglin, C., Sun, Y. L., Tian, J., Laaksonen, A., Raatikainen, T., Rautiainen, J., Vaattovaara, P., Ehn, M., Kulmala, M., Tomlinson, J. M., Collins, D. R., Cubison, M. J., Dunlea, E. J., Huffman, J. A., Onasch, T. B., Alfarra, M. R., Williams, P. I., Bower, K., Kondo, Y., Schneider, J., Drewnick, F., Borrmann, S., Weimer, S., Demerjian, K., Salcedo, D., Cottrell, L., Griffin, R., Takami, A., Miyoshi, T., Hatakeyama, S., Shimono, A., Sun, J. Y., Zhang, Y. M., Dzepina, K., Kimmel, J. R., Sueper, D., Jayne, J. T., Herndon, S. C., Trimborn, A. M., Williams, L. R., Wood, E. C., Middlebrook, A. M., Kolb, C. E., Baltensperger, U., and Worsnop, D. R.: Evolution of organic aerosols in the atmosphere, Science, 326, 1525–1529, doi:10.1126/science.1180353, 2009.
Juranyi, Z., Gysel, M., Duplissy, J., Weingartner, E., Tritscher, T., Dommen, J., Henning, S., Ziese, M., Kiselev, A., Stratmann, F., George, I., and Baltensperger, U.: Influence of gas-to-particle partitioning on the hygroscopic and droplet activation behaviour of alpha-pinene secondary organic aerosol, Phys. Chem. Chem. Phys., 11, 8091–8097, doi:10.1039/B904162a, 2009.
Knopf, D. A.: Thermodynamic properties and nucleation processes of upper tropospheric and lower stratospheric aerosol particles, Diss. ETH No. 15103, Zurich, Switzerland, 2003.
Koop, T., Kapilashrami, A., Molina, L. T., and Molina, M. J.: Phase transitions of sea-salt/water mixtures at low temperatures: implications for ozone chemistry in the polar marine boundary layer, J. Geophys. Res.-Atmos., 105, 26393–26402, doi:10.1029/2000jd900413, 2000.
Krieger, U. K., Marcolli, C., and Reid, J. P.: Exploring the complexity of aerosol particle properties and processes using single particle techniques, Chem. Soc. Rev., 41, 6631–6662, doi:10.1039/c2cs35082c, 2012.
Kuwata, M. and Martin, S. T.: Phase of atmospheric secondary organic material affects its reactivity, P. Natl. Acad. Sci. USA, 109, 17354–17359, doi:10.1073/pnas.1209071109, 2012.

ACPD
15, 33379–33405, 2015

Liu, P. F., Zhang, Y., and Martin, S. T.: Complex refractive indices of thin films of secondary organic materials by spectroscopic ellipsometry from 220 to 1200 nm, Environ. Sci. Technol., 47, 13594–13601, doi:10.1021/Es403411e, 2013.
Martin, S. T.: Phase transitions of aqueous atmospheric particles, Chem. Rev., 100, 3403–3453, doi:10.1021/Cr990034t, 2000.
Massoli, P., Lambe, A. T., Ahern, A. T., Williams, L. R., Ehn, M., Mikkila, J., Canagaratna, M. R., Brune, W. H., Onasch, T. B., Jayne, J. T., Petaja, T., Kulmala, M., Laaksonen, A., Kolb, C. E., Davidovits, P., and Worsnop, D. R.: Relationship between aerosol oxidation level and hygroscopic properties of laboratory generated secondary organic aerosol (SOM) particles, Geophys. Res. Lett., 37, L24801, doi:10.1029/2010gl045258, 2010.
Pajunoja, A., Lambe, A. T., Hakala, J., Rastak, N., Cummings, M. J., Brogan, J. F., Hao, L. Q., Paramonov, M., Hong, J., Prisle, N. L., Malila, J., Romakkaniemi, S., Lehtinen, K. E. J., Laaksonen, A., Kulmala, M., Massoli, P., Onasch, T. B., Donahue, N. M., Riipinen, I., Davidovits, P., Worsnop, D. R., Petaja, T., and Virtanen, A.: Adsorptive uptake of water by semisolid secondary organic aerosols, Geophys. Res. Lett., 42, 3063–3068, doi:10.1002/2015gl063142, 2015.
Pankow, J. F.: Gas/particle partitioning of neutral and ionizing compounds to single and multi-phase aerosol particles. 1. Unified modeling framework, Atmos. Environ., 37, 3323–3333, doi:10.1016/S1352-2310(03)00346-7, 2003.
Pant, A., Parsons, M. T., and Bertram, A. K.: Crystallization of aqueous ammonium sulfate particles internally mixed with soot and kaolinite: crystallization relative humidities and nucleation rates, J. Phys. Chem. A, 110, 8701–8709, doi:10.1021/Jp060985s, 2006.
Parsons, M. T., Knopf, D. A., and Bertram, A. K.: Deliquescence and crystallization of ammonium sulfate particles internally mixed with water-soluble organic compounds, J. Phys. Chem. A, 108, 11600–11608, doi:10.1021/Jp0462862, 2004.
Petters, M. D. and Kreidenweis, S. M.: A single parameter representation of hygroscopic growth and cloud condensation nucleus activity, Atmos. Chem. Phys., 7, 1961–1971, doi:10.5194/acp-7-1961-2007, 2007.
Petters, M. D., Kreidenweis, S. M., Snider, J. R., Koehler, K. A., Wang, Q., Prenni, A. J., and Demott, P. J.: Cloud droplet activation of polymerized organic aerosol, Tellus B, 58, 196–205, doi:10.1111/j.1600-0889.2006.00181.x, 2006.
Petters, M. D., Wex, H., Carrico, C. M., Hallbauer, E., Massling, A., McMeeking, G. R., Poulain, L., Wu, Z., Kreidenweis, S. M., and Stratmann, F.: Towards closing the gap be-

ACPD
15, 33379–33405, 2015

tween hygroscopic growth and activation for secondary organic aerosol – Part 2: Theoretical approaches, Atmos. Chem. Phys., 9, 3999–4009, doi:10.5194/acp-9-3999-2009, 2009.

Poschl, U., Martin, S. T., Sinha, B., Chen, Q., Gunthe, S. S., Huffman, J. A., Borrmann, S., Farmer, D. K., Garland, R. M., Helas, G., Jimenez, J. L., King, S. M., Manzi, A., Mikhailov, E., Pauliquevis, T., Petters, M. D., Prenni, A. J., Roldin, P., Rose, D., Schneider, J., Su, H., Zorn, S. R., Artaxo, P., and Andreae, M. O.: Rainforest aerosols as biogenic nuclei of clouds and precipitation in the Amazon, Science, 329, 1513–1516, doi:10.1126/science.1191056, 2010.

Prenni, A. J., Petters, M. D., Kreidenweis, S. M., DeMott, P. J., and Ziemann, P. J.: Cloud droplet activation of secondary organic aerosol, J. Geophys. Res.-Atmos., 112, D10223, doi:10.1029/2006jd007963, 2007.

Prenni, A. J., Petters, M. D., Kreidenweis, S. M., Heald, C. L., Martin, S. T., Artaxo, P., Garland, R. M., Wollny, A. G., and Poschl, U.: Relative roles of biogenic emissions and Saharan dust as ice nuclei in the Amazon basin, Nat. Geosci., 2, 401–404, doi:10.1038/Ngeo517, 2009.

Raymond, T. M. and Pandis, S. N.: Cloud activation of single-component organic aerosol particles, J. Geophys. Res.-Atmos., 107, 4787, doi:10.1029/2002jd002159, 2002.

Saunders, S. M., Jenkin, M. E., Derwent, R. G., and Pilling, M. J.: Protocol for the development of the Master Chemical Mechanism, MCM v3 (Part A): tropospheric degradation of non-aromatic volatile organic compounds, Atmos. Chem. Phys., 3, 161–180, doi:10.5194/acp-3-161-2003, 2003.

Shrestha, M., Zhang, Y., Ebben, C. J., Martin, S. T., and Geiger, F. M.: Vibrational sum frequency generation spectroscopy of secondary organic material produced by condensational growth from alpha-pinene ozonolysis, J. Phys. Chem. A, 117, 8427–8436, doi:10.1021/Jp405065d, 2013.

Song, M., Marcolli, C., Krieger, U. K., Zuend, A., and Peter, T.: Liquid-liquid phase separation and morphology of internally mixed dicarboxylic acids/ammonium sulfate/water particles, Atmos. Chem. Phys., 12, 2691–2712, doi:10.5194/acp-12-2691-2012, 2012.

Song, M., Liu, P. F., Hanna, S. J., Li, Y. J., Martin, S. T., and Bertram, A. K.: Relative humidity-dependent viscosities of isoprene-derived secondary organic material and atmospheric implications for isoprene-dominant forests, Atmos. Chem. Phys., 15, 5145–5159, doi:10.5194/acp-15-5145-2015, 2015.

ACPD
15, 33379–33405, 2015

Wex, H., Hennig, T., Salma, I., Ocskay, R., Kiselev, A., Henning, S., Massling, A., Wiedensohler, A., and Stratmann, F.: Hygroscopic growth and measured and modeled critical super-saturations of an atmospheric HULIS sample, Geophys. Res. Lett., 34, L02818, doi:10.1029/2006GL028260, 2007.

Wex, H., Topping, D., McFiggans, G., and Stratmann, F.: The Kelvin versus the Raoult term in the Köhler equation, J. Atmos. Sci., 65, 4004–4016, doi:10.1175/2008JAS2720.1, 2008.

You, Y., Renbaum-Wolff, L., Carreras-Sospedra, M., Hanna, S. J., Hiranuma, N., Kamal, S., Smith, M. L., Zhang, X. L., Weber, R. J., Shilling, J. E., Dabdub, D., Martin, S. T., and Bertram, A. K.: Images reveal that atmospheric particles can undergo liquid–liquid phase separations, P. Natl. Acad. Sci. USA, 109, 13188–13193, doi:10.1073/pnas.1206414109, 2012.

You, Y., Smith, M. L., Song, M. J., Martin, S. T., and Bertram, A. K.: Liquid–liquid phase separation in atmospherically relevant particles consisting of organic species and inorganic salts, Int. Rev. Phys. Chem., 33, 43–77, doi:10.1080/0144235X.2014.890786, 2014.

Zhang, Q., Jimenez, J. L., Canagaratna, M. R., Allan, J. D., Coe, H., Ulbrich, I., Alfarra, M. R., Takami, A., Middlebrook, A. M., Sun, Y. L., Dzepina, K., Dunlea, E., Docherty, K., DeCarlo, P. F., Salcedo, D., Onasch, T., Jayne, J. T., Miyoshi, T., Shimono, A., Hatakeyama, S., Takegawa, N., Kondo, Y., Schneider, J., Drewnick, F., Borrmann, S., Weimer, S., Demerjian, K., Williams, P., Bower, K., Bahreini, R., Cottrell, L., Griffin, R. J., Rautiainen, J., Sun, J. Y., Zhang, Y. M., and Worsnop, D. R.: Ubiquity and dominance of oxygenated species in organic aerosols in anthropogenically-influenced Northern Hemisphere midlatitudes, Geophys. Res. Lett., 34, L13801, doi:10.1029/2007gl029979, 2007.

Zuend, A. and Seinfeld, J. H.: Modeling the gas-particle partitioning of secondary organic aerosol: the importance of liquid-liquid phase separation, Atmos. Chem. Phys., 12, 3857–3882, doi:10.5194/acp-12-3857-2012, 2012.

Zuend, A. and Seinfeld, J. H.: A practical method for the calculation of liquid–liquid equilibria in multicomponent organic–water–electrolyte systems using physicochemical constraints, Fluid Phase Equilibr., 337, 201–213, 2013.

Zuend, A., Marcolli, C., Luo, B. P., and Peter, T.: A thermodynamic model of mixed organic-inorganic aerosols to predict activity coefficients, Atmos. Chem. Phys., 8, 4559–4593, doi:10.5194/acp-8-4559-2008, 2008.

ACPD
15, 33379–33405, 2015

Zuend, A., Marcolli, C., Peter, T., and Seinfeld, J. H.: Computation of liquid-liquid equilibria and phase stabilities: implications for RH-dependent gas/particle partitioning of organic-inorganic aerosols, Atmos. Chem. Phys., 10, 7795–7820, doi:10.5194/acp-10-7795-2010, 2010.

Zuend, A., Marcolli, C., Booth, A. M., Lienhard, D. M., Soonsin, V., Krieger, U. K., Topping, D. O., McFiggans, G., Peter, T., and Seinfeld, J. H.: New and extended parameterization of the thermodynamic model AIOMFAC: calculation of activity coefficients for organic-inorganic mixtures containing carboxyl, hydroxyl, carbonyl, ether, ester, alkenyl, alkyl, and aromatic functional groups, Atmos. Chem. Phys., 11, 9155–9206, doi:10.5194/acp-11-9155-2011, 2011.

ACPD
15, 33379–33405, 2015

Table 1. Summary of experimental conditions for the production and collection of α-pinene-derived SOM. SOM samples 2, 3, 4, 5, 7, and 8 were collected on hydrophobic substrates using a single stage impactor. SOM samples 1, 6, and 9 were collected on hydrophobic substrates using an electrostatic precipitator. The separation relative humidity (SRH) from one to two phases is listed for each SOM. The standard deviation (SD) is derived from several cycles of RH for different deposited particles. In cases for which the SRH was only determined for one humidity cycle (SOM samples 3–5), the error represents the maximum error reported for the other SOM samples. SOM particle mass concentration refers to the concentration of organic particles suspended in the gas phase at the time of SOM production.

SOM sample	α-pinene (ppm)	O_3 (ppm)	SOM particle mass concentration ($\mu g\,m^{-3}$)	Collection time (min)	SRH (%) ± SD with decreasing RH	SRH (%) ± SD with increasing RH
1	0.20	16	75	3120	96.2 ± 0.41	96.4 ± 0.03
2	0.35	10	85	5580	95.8 ± 0.18	95.9 ± 0.04
3	0.35	10	95	5733	95.1 ± 0.41	95.2 ± 0.41
4	0.35	10	110	2160	94.7 ± 0.13	95.0 ± 0.41
5	0.80	10	320	1590	95.2 ± 0.41	96.3 ± 0.41
6	1.00	20	1500	1440	96.2 ± 0.39	96.1 ± 0.08
7	5.00	10	2900	1520	97.3 ± 0.08	96.7 ± 0.39
8	5.00	10	2900	1472	95.8 ± 1.05	96.5 ± 0.21
9	5.00	20	11 000	330	96.5 ± 0.23	96.5 ± 0.28

ACPD
15, 33379–33405, 2015

Table 2. Molecular weights (M_w), O : C ratios and mole fractions of the α-pinene ozonolysis products from Zuend and Seinfeld (2012) used in the thermodynamic modelling study. Three different scenarios were investigated: high SOM concentrations (SOM-high), low SOM concentration (SOM-low) and with higher shares of the more oxidized products (SOM-ox).

Name	M_w ($g\,mol^{-1}$)	O : C	Mole fraction in mixture		
			SOM-high	SOM-low	SOM-ox
C107OOH	200.231	0.4	0.039	0.013	0.009
Pinonic acid	184.232	0.3	0.016	0.000	0.000
C97OOH	188.221	0.444	0.310	0.042	0.030
C108OOH	216.231	0.5	0.050	0.012	0.009
ALDOL_dimer	368.421	0.368	0.029	0.079	0.056
Pinic acid	186.205	0.444	0.167	0.156	0.110
C921OOH	204.220	0.556	0.138	0.271	0.192
C109OOH	200.231	0.4	0.005	0.000	0.000
C812OOH	190.194	0.625	0.128	0.277	0.245
ESTER_dimer	368.421	0.368	0.005	0.021	0.015
C811OH	158.094	0.375	0.012	0.000	0.000
Hopinonic acid	200.232	0.4	0.058	0.026	0.019
C813OOH	206.193	0.75	0.042	0.102	0.316

ACPD
15, 33379–33405, 2015

Table 3. Calculated properties of the mixtures SOM-high, SOM-low and SOM-ox: average O : C ratio; average molecular weight; range of LLPS for a 20 µm particle in diameter; critical supersaturation SSc for a 100 nm particle, κ_{HGF} from the hygroscopic growth curve at 90 % RH for a 100 nm diameter particle, κ_{CCN} from SSc of the Köhler curve for a 100 nm particle, simulated mass yields at 60 % RH reported in Zuend and Seinfeld (2012).

	SOM-high	SOM-low	SOM-ox
av. O : C	0.472	0.513	0.582
av. M ($g\,mol^{-1}$)	199.5	213.5	210.6
LLPS range (% RH)	99.31–99.88	98.91–99.94	98.71–99.92
SSc (%)	1.206	0.624	0.420
κ_{HGF} at 90 % RH	0.0252	0.0303	0.0334
κ_{CCN}	0.0093	0.0364	0.0803
PM mass conc. ($\mu g\,m^{-3}$)	21.86	0.81	–

ACPD
15, 33379–33405, 2015

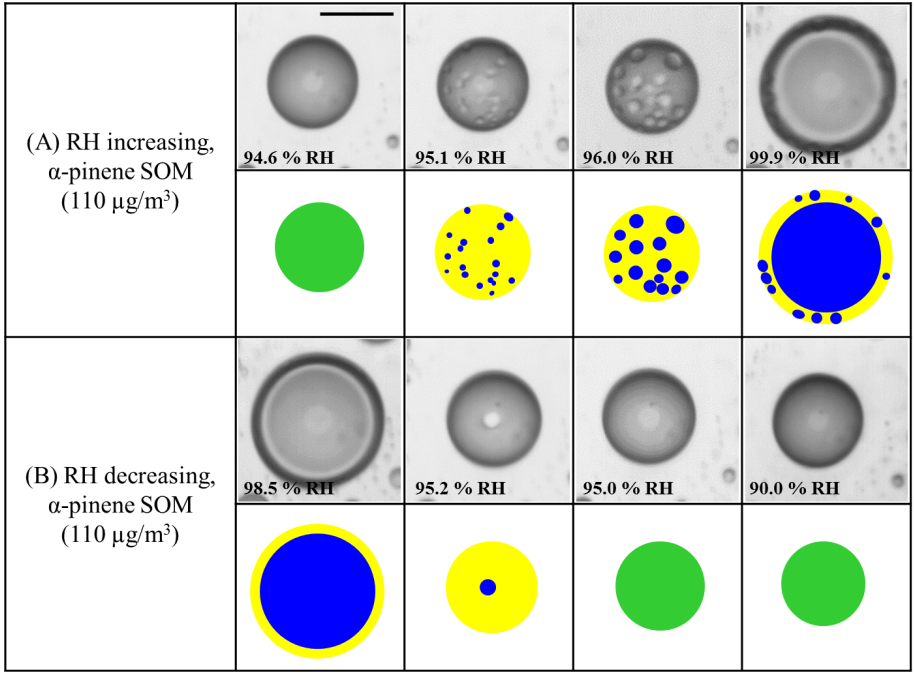

Figure 1. Effect of RH cycles on α-pinene-derived SOM for SOM produced at 110 µg m^{-3}. Illustrations of the images are shown for clarity. Green: SOM + water. Yellow: SOM-rich phase. Blue: water-rich phase. Size bar is 20 µm.

ACPD
15, 33379–33405, 2015

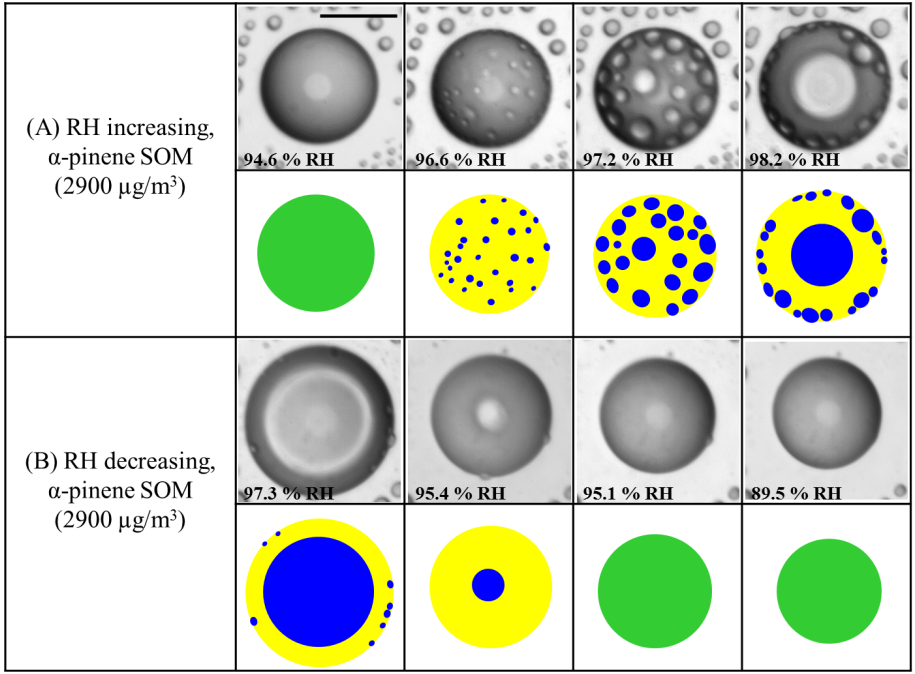

Figure 2. Effect of RH cycles on α-pinene-derived SOM for SOM produced at 2900 µg m^{-3}. Illustrations of the images are shown for clarity. Green: SOM + water. Yellow: SOM-rich phase. Blue: water-rich phase. Size bar is 20 µm.

ACPD
15, 33379–33405, 2015

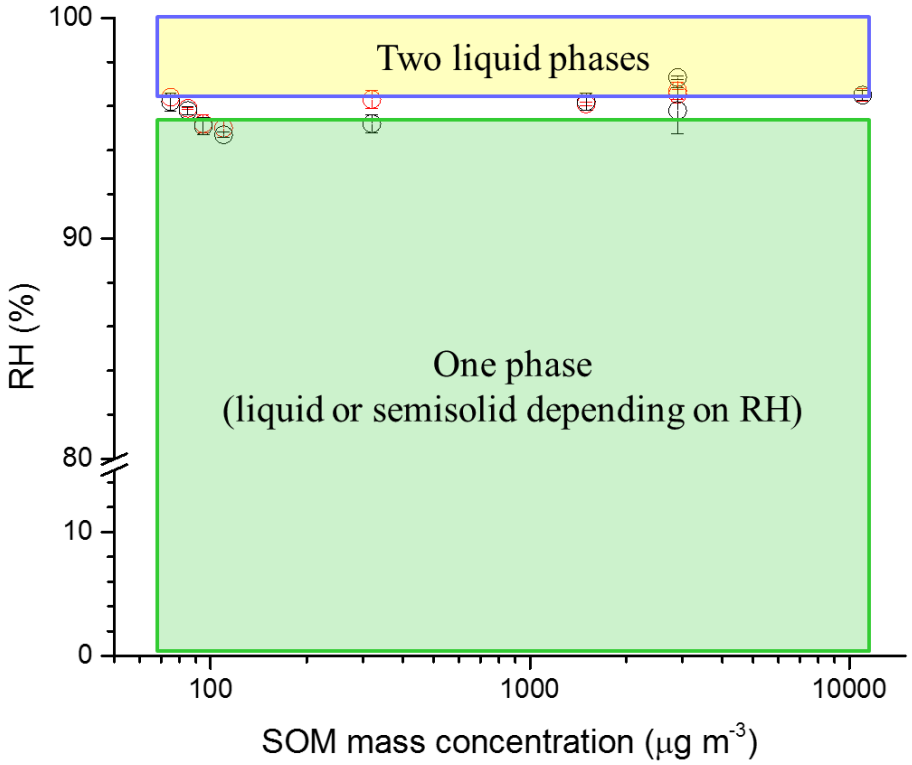

Figure 3. Relative humidity (RH) at which phase transition between one phase and two liquid phases was observed for α-pinene-derived SOM as a function of the mass concentration of SOM produced. Red circles: onset of phase separation upon moistening. Black circles: merging of the two liquid phases upon drying. The y-error bars represent the standard deviation in RH determination at the phase transition. Green shaded region: one phase (liquid or semisolid depending on RH) prevalent in α-pinene-derived SOM. Yellow shaded region: two liquid phases present.

ACPD
15, 33379–33405, 2015

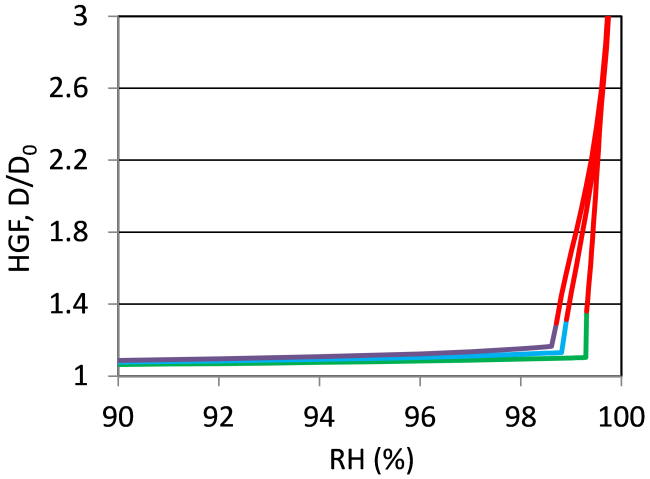

Figure 4. Simulated hygroscopic growth factors HGF = D/D_0 for SOM-high (green, O : C = 0.472), SOM-low (blue, O : C = 0.513) and SOM-ox (purple, O : C = 0.582) for a dry diameter of 20 µm, which is similar in size to the particles used in the optical microscope experiments. The red segments on the lines indicate the presence of LLPS.

ACPD
15, 33379–33405, 2015

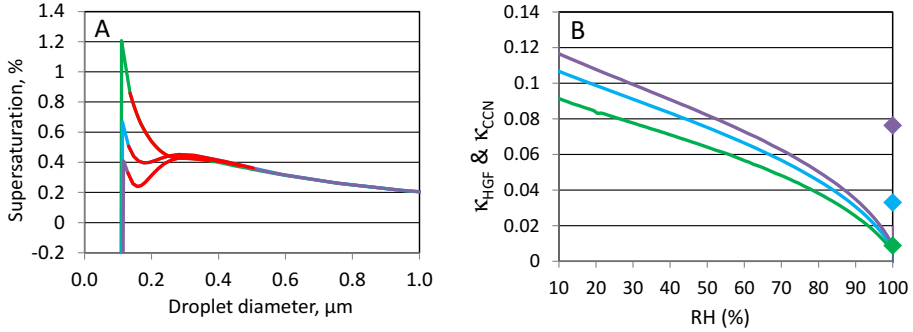

Figure 5. Köhler curves (Panel A) and hygroscopicity parameter κ (Panel B) for a particle with a dry diameter of 100 nm for SOM-high (green, O : C = 0.472), SOM-low (blue, O : C = 0.513) and SOM-ox (purple, O : C = 0.582). The red segments on the lines in Panel **(a)** indicate the presence of LLPS. In panel **(b)**, κ_{HGF} is given as solid line as a function of RH and κ_{CCN} as diamond at RH = 100 %.

ACPD
15, 33379–33405, 2015